2023

A Study of the Performance of Wind Turbines Fitted with Sprayed Liquid Flaps

Alexander Spitzer
University of Central Florida

A STUDY OF THE PERFORMANCE OF WIND TURBINES FITTED WITH SPRAYED LIQUID FLAPS

By

ALEXANDER LESLIE SPITZER
B.S University of Central Florida, 2021

A thesis submitted in partial fulfillment of the requirements
for the degree of Master of Science
in the Department of Mechanical and Aerospace Engineering
in the College of Engineering and Computer Science
at the University of Central Florida
Orlando, Florida

Summer Term
2023

ABSTRACT

Lift generating technologies are often considered a potential solution to increased power generation and reliability within wind turbine design. The Sprayed Liquid Flap (SLF) is a novel active control method that has shown success in providing lift generation on aircraft wings, but its application in the context of rotating flows is unexplored. This research aims to understand the effects of the SLF on a wind turbine and provide a pathway for future exploration of its aerodynamic impacts on rotating flows. Computational Fluid Dynamics with an Euler-Euler multiphase approach is employed to assess the influence of the SLF on a wind turbine's power generation capabilities. With the need for multiphase physics comes increased computational cost which poses a challenge for future research into the rotational multiphase flows. The Blade Element Momentum Method (BEM) provides an elegant, proven solution for estimating rotating flows for cheap so to aid in future works, the efficacy of BEM as an estimator for multiphase rotating flows will be explored through a SLF equipped wind turbine. The current findings indicate that the SLF equipped wind turbine exhibits power benefits over a conventional turbine. In addition, they suggest that BEM could serve as a reasonable estimator for the exploration of rotational multiphase physics.

ACKNOWLEDGEMENTS

I would like to express my gratitude to my graduate advisor and chair Dr. Michael Kinzel for his continued investment in my success. His guidance in computational fluid dynamics and extensive support were critical for the development of this work.

I would also like to thank Dr. George Loubimov for his advice and constructive feedback during the development and continuation of this research.

TABLE OF CONTENTS

LIST OF FIGURES

LIST OF TABLES

CHAPTER 1: INTRODUCTION

Wind energy in the U.S has received large additions to capacity within the last decade. Figure 1 from the 2022 Land-Based Wind Market Report published by the U.S. Department of Energy plots the cumulative total capacity and annual capacity of wind energy in the U.S. since 1998. 2021 was among the top 3 years of annual capacity generation in the U.S. but wind penetration, a measure of wind capacity against total capacity of all energy forms, was only 9.1%. As suggested by reference [1], the future success of the wind energy sector is largely dependent on its economic position compared to other resources. Therefore, the ability to achieve increased performance for cheap proves to be one of the main challenges keeping wind energy from increasing penetration. Computational Fluid Dynamics (CFD) simulations are a standard tool used by turbine designers to estimate the performance of potential turbine options. The Blade Element Momentum Method is often a solution for wind turbine designers to explore potential designs with little comparative computational cost [2].

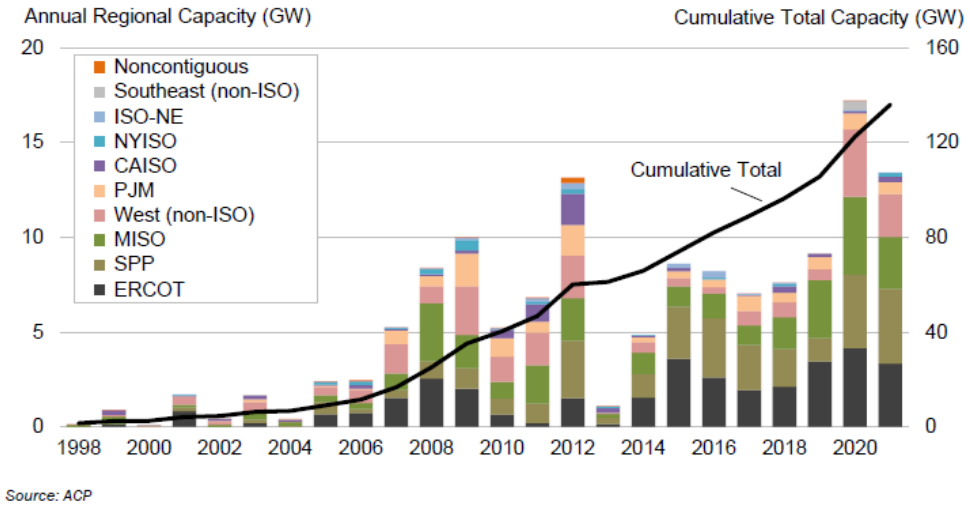

Figure 1: 2022 U.S Wind Power Capacity Report [1]

BEM not only provides cheap understanding of conventional turbine designs but also provides an economical avenue for the exploration of rotational power generating devices. One such power generating technology is the Sprayed Liquid Flap (SLF). Previously studied on 3D finite wings [3,4], the novel mechanical flap alternative provides a boost in lift over drag performance by jettisoning an atomized fluid from the pressure surface of the airfoil. While its benefits were computationally shown on wings, its multiphase effects have yet to be explored in a rotational context. This thesis aims to determine the performance of a SLF equipped wind turbine and the effectiveness of BEM as a pathway for future cheap rotational multiphase research.

CHAPTER 2: AN EVALUATION OF A SPRAYED LIQUID FLAP ON A 3D WIND TURBINE BLADE

The information contained within this chapter was previously published by AIAA at the SciTech 2023 national conference held in National Harbor. See reference [5] for the past publication.

Abstract

Previous studies found that the Sprayed Liquid Flap (SLF) can be modeled using potential flow as an alternative to three-dimensional, multiphase, Computational Fluid Dynamics (CFD). The objective of this chapter is to expand on these previous studies by examining the SLF in the context of rotating flows such as wind turbines. CFD simulations will be used to determine the effectiveness of the Blade Element Momentum Method as an estimator for a wind turbine equipped with a sprayed liquid flap. Once this method is validated the power, thrust, and torque coefficients of cases with and without the sprayed liquid flap will be compared so conclusions can be drawn.

Nomenclature

TSR	=	Tip Speed Ratio
SLF	=	Sprayed Liquid Flap
FR	=	Fully Resolved
BEM	=	Blade Element Momentum Method
α	=	Angle of Attack
C_P	=	Power Coefficient
C_T	=	Thrust Coefficient
C_Q	=	Torque Coefficient
c	=	Chord
s	=	Span

2.1 Introduction

Wind Turbine designers are consistently aiming to increase the power generation of turbines at lower cost. One avenue is to increase the reliability of the turbines, that is reduce the necessary structure of a wind turbine blade by reducing its expected peak loads. This is where powered lift concepts can help, by providing load control that mitigates high loading events to reduce the demands of the structure [6]. The normal approach to increase efficiency is through blade optimization, but such optimization cannot consider adverse events. Hence, load control is attractive as it mitigates the loads in the peak loading condition enabling the relaxation of the structural design. In addition, there are possibilities for these devices to also improve the performance of a wind turbine. Like lift generating devices being used to increase flight envelopes in wing design, lift generating devices are important in increasing a wind turbines ability to generate power at an increased range of conditions. Lift generating devices, like flaps, have been widely commercialized due to their ability to increase lift during takeoff and landing when flight speeds are reduced.

The Sprayed Liquid Flap (SLF), example shown in Figure 2, has been proved to function as a lift generating device in wing design [4] but its behavior within a rotating reference frame has yet to be assessed. If the SLF functions similarly in a rotating reference frame as it did within wing design, it could provide designers with a new addressable method of increasing lift at given conditions. Increasing lift at a given condition could potentially translate to an increase in power generation range. While the SLF might have the ability to improve wind turbine reliability, simulating its effects is computationally expensive. The simulation of the SLF requires the use of Euler-Euler physics which has a significant impact on computational cost. To accurately predict

the lift-generating physics, sufficient resolution is required to capture the interaction between freestream and injected spray which drives computational cost. One cost-saving method previously explored was the combination of 2D CFD simulations with lifting line theory in lieu of fully resolved 3D CFD [3]. In Ref. [3], it was found that finite wing equipped with a SLF behaved in accordance with conventional aerodynamic theory and was well suited to be modeled with lifting line theory and 2D CFD. This finding leads to the hypothesis that modeling the SLF in a rotational reference frame using Blade Element Momentum (BEM) techniques can also be successful.

To validate this hypothesis, several numerical assessments will be conducted and are outlined as follows. First, a benchmarking assessment is conducted by comparing numerical results to the NREL 5MW Wind Turbine [7] to quantify the numerical uncertainty. Next, a comparison between fully resolved, 3D CFD simulations of the SLF are compared against a BEM approach is conducted to determine if this modeling approach is sufficient for parameter exploration. Finally, some comparisons between a simplified wind-turbine blade and a SLF-equipped blade are made to drive a qualitative discussion of the benefits of the SLF technology.

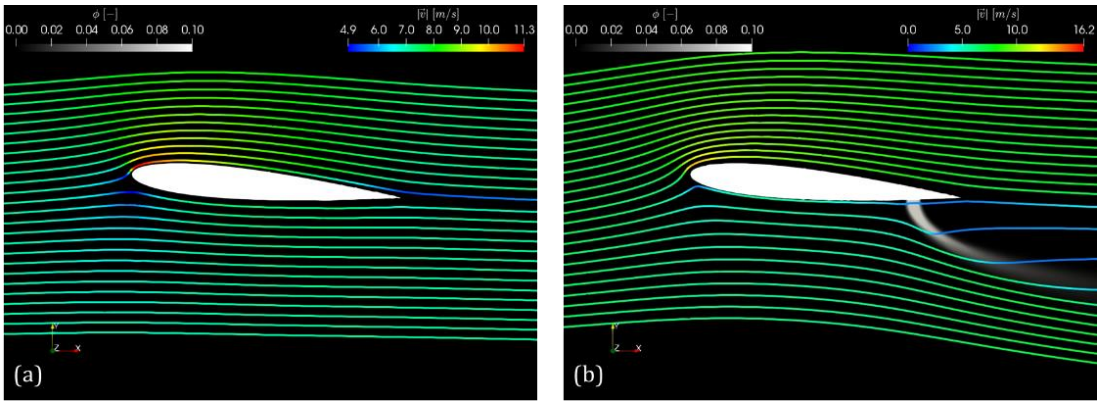

Figure 2: Flow visualization of NACA 0012 airfoil showing streamlines colored by velocity magnitude Part (a) shows the conventional foil and part (b) shows an active SLF [4]

2.2 Methods

2.2.1 Euler-Euler Approach

The present study analyzes the underlying aerodynamic response of a powered-lift device involving two-phase flow using CFD [8]. The physical assumptions can be generally described as: steady, Newtonian, turbulent, isothermal, and incompressible flow. The multiphase aspect of the model is treated using a two-way coupled Euler-Euler approach. An underlying assumption is that of the atomization processes which are not directly resolved. Instead, a consistent and uniform droplet diameter was assumed. Such an assumption is not limiting, but rather would be associated with complex processes and designs associated with the liquid jet mechanisms. The physical model considers interactions associated with drag and buoyancy forces acting on the liquid droplets.

The Eulerian-Eulerian model equations are driven on mass, momentum, and turbulence modeling. For the gas flow, the representative equations for mass and momentum balance equations are, respectively, given as

$$\frac{\partial \overline{u_\iota}}{\partial x_i} = 0$$

and

$$\frac{\partial \overline{u_\iota}}{\partial t} + \frac{\partial \overline{u_\iota}\,\overline{u_\jmath}}{\partial x_i} = -\frac{1}{\rho}\frac{\partial \bar{p}}{\partial x_i} + \frac{1}{\rho}\frac{\partial}{\partial x_i}\left((\mu + \mu_t)\frac{\partial\,\overline{u_\iota}}{\partial x_i}\right) - F_{l,i}^{d}.$$

Here, $\overline{u_\iota}$ is the gas velocity vector, x_i is the Cartesian spatial coordinate, $\bar{p}$ is pressure, μ is the viscosity, and μ_t is the eddy viscosity (or turbulence) model. The $F_{l,i}^{d}$ term is the momentum

exchange the droplets provide with the gaseous phase and will be discussed in additional detail below. The Spalart-Allmaras turbulence model is used to model the turbulent eddy viscosity, μ_t:

$$\mu_t = \rho f_{v1} \tilde{v}$$

Where f_{v1}represents a damping function. The modified diffusivity, $\tilde{v}$, is solved using a transport equation:

$$\frac{\partial \rho \tilde{v} \bar{u}_i}{\partial x_i} = \frac{1}{\sigma_{\tilde{v}}} \frac{\partial}{\partial x_i} \left[(\mu + \tilde{v}) \frac{\partial \tilde{v}}{\partial x_i} \right] + P_{\tilde{v}} + S_{\tilde{v}}$$

The representative equations for the atomized liquid droplets represent a dilute droplet phase that is not continuous and is driven by interactions with the gas. In a Euler-Euler approach, droplet mass is conserved through conserving the liquid volume which introduces the liquid volume fraction, ϕ. The conservation equations for liquid are for mass and momentum are, respectively, given as:

$$\frac{\partial \rho_l \phi}{\partial t} + \frac{\partial \rho_l \phi u_{l.i}}{\partial x_i} = 0$$

and

$$\frac{\partial u_{l,j}}{\partial t} + \frac{\partial u_{l,i} u_{l,j}}{\partial x_i} = -\frac{1}{\rho} \frac{\partial p}{\partial x_i} + F_{l,i}^d.$$

In these equations, ρ_l is the liquid density, $u_{l.i}$ is the liquid velocity, p is the static pressure (shared with the gaseous phase), and $F_{l,i}^d$ is the drag force vector that acts on the liquid dispersed phase due to the drag of gas phase. The primary interactions between the gas and liquid droplets are given through the drag force that is given as:

$$F_l^d = \frac{1}{2} C_{D_l} \left(\frac{6\phi}{4D}\right) \rho_l |\overline{u}_r| \overline{u}_r,$$

where $\overline{u}_r$ is the relative velocity between the dispersed and continuous phase ($\overline{u}_r = \overline{u}_l - \overline{u}$). The drag coefficient, C_{D_l}, of the droplets is based on the Schiller-Naumann model given as:

$$C_D = \begin{cases} \frac{24}{Re_p}(1 + \frac{1}{6} Re_p^{\frac{2}{3}}), & Re_p \leq 1000 \\ 0.424 \quad , & Re_p \geq 1000 \end{cases}.$$

The droplet Reynolds number, Re_p, is calculated using:

$$Re_p = \frac{\rho_l |\overline{u}_r| D_l}{\mu_l}.$$

where ρ_l and $\mu_l$are the density and the dynamic viscosity of the mixture, respectively. These properties are calculated via volume weighting.

2.2.2 Rotating Reference Frame

To simulate rotation of the wind turbine blades in StarCCM+, a rotating reference frame was used. This method, also referred to as the frozen rotor approach, provides a constant mass flux term to the conservation equations from the effects of the region rotating around the body [6,9]. This approach, an alternative to rigid body motion, mitigates the computational cost associated with moving the mesh vertices between timesteps. Instead, through the constant rotation of the region's reference frame, the time-averaged behaviors can be investigated using steady solvers.

To further mitigate costs associated with mesh vertices, rotational periodic boundary conditions were used ahead and behind the turbine on its rotational plane. The domain geometry and boundary conditions can be seen in Figure 6. These conditions link the flow information of one boundary to another. Since the turbine being explored uses 3 blades, the entire cylindrical domain is split into 3 equal 120-degree sections each including a single blade. This effectively simulates a 3-blade turbine with a third the cost.

2.2.3 Blade Element Momentum Method

The Blade Element Method couples with CFD to connect two-dimensional airfoil aerodynamics into three-dimensional momentum within a virtual disk. It is a two-step process in which an interpolation grid is created and then momentum source terms for each element within the grid are calculated based on inflow characteristics and effective angles of attack which are passed through additionally required 2D aerodynamic airfoil tables provided to the model [10] . The interpolation grid is the defining factor for computational cost with BEM. The generated interpolation grid must have at least one full mesh cell within each of its elements. This is because the mesh cells within each element are provided momentum terms consistent with the forces generated at the location data of each grid element. The forces of each element are calculated by:

$$D = \frac{1}{2}\rho v'^{2} C_d c \cdot ds$$

$$L = \frac{1}{2}\rho v'^{2} C_l c \cdot ds$$

Where v' is:

$$v' = \sqrt{\left(v_{tangential}\right)^2 + (v_{axial})^2}$$

The forces are transposed into the lab coordinate frame and are then imposed on the fluid. Since the blade only acts within a part of the total area covered by the BEM interpolation grid, the resultant force is scaled by a time fraction:

$$S = \frac{b\Delta\varphi}{2\pi}$$

Where b is the number of blades. This provides a reasonably accurate method to quickly assess the aerodynamics of the wind turbine in complex scenarios. While BEM is often used for the evaluation of wind turbines[11], its efficacy as an estimator for the rotational multiphase associated with an SLF equipped wind turbine will be discussed below.

2.3 Results

2.3.1 3D Lifting Line Theory

Based on the previous work of Loubimov[3] , it was shown that Lifting Line Theory (LLT) could predict the three-dimensional lift curve of a SLF equipped airfoil through 2D CFD. Figure 3 shows the results of a LLT model compared with 3D CFD. Part (a) plots sectional lift coefficient against normalized span. In the 3D CFD data, as the position along the normalized span increased, the sectional lift coefficient rapidly drops off due to the tip effects of the wing. Similar tip effects can be seen in the LLT data as the model closely matches the 3D CFD curve. Part (b) of Figure 3 plots the total lift coefficient of the wing against angles of attack within the linear two Pi alpha

range of angles. The LLT data shows a negative bias compared to the 3D CFD and does a good job of capturing the linear trend. These results suggest that SLF equipped foils are affected by induced flow in the same manner as conventional wings. This evidence suggests that using potential flow to model the SLF in a rotating frame is within reason.

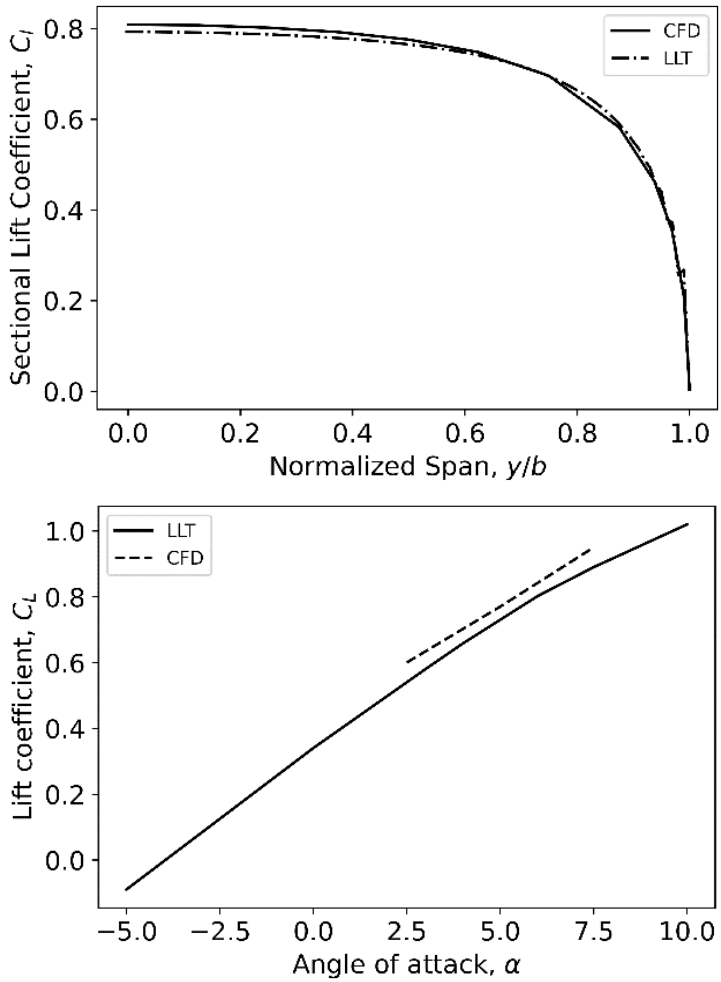

Figure 3: Comparison of CFD and LLT of SLF Equipped Airfoils - (a) Sectional Lift Coefficient vs Normalized Span, (b) Lift Coefficient vs Angle of Attack

2.3.2 QBlade Rotor BEM Validation

To determine the validity of QBlade[12] Rotor BEM, a copy of the NREL 5MW turbine blade was modeled in QBlade and results were coplotted against the published NREL results from FAST[7]. Figure 5 shows the coplotted results. Limited data of wind speeds ranging from 3m/s to 11.4 m/s was investigated since the previously published results applied a pitch varying trimming method to speeds above the rated operating condition of 11.4m/s. There were differences between the blades used in this exploration. The NREL blade uses cylindrical foils near the root but, nodes 1-3 of the QBlade blade were replaced with DU-40 airfoils which have different lift characteristics as compared to the cylinders. Figure 4 shows the node positions for each station of the blade and their respective airfoil. Likely due to this change and the additional data required by FAST as a higher fidelity solver compared to QBlade, the power and torque estimates made by QBlade are overestimated by about 24.29% difference. Regardless of this change, the resultant power, torque, and thrust are following similar trends as the previously published FAST data.

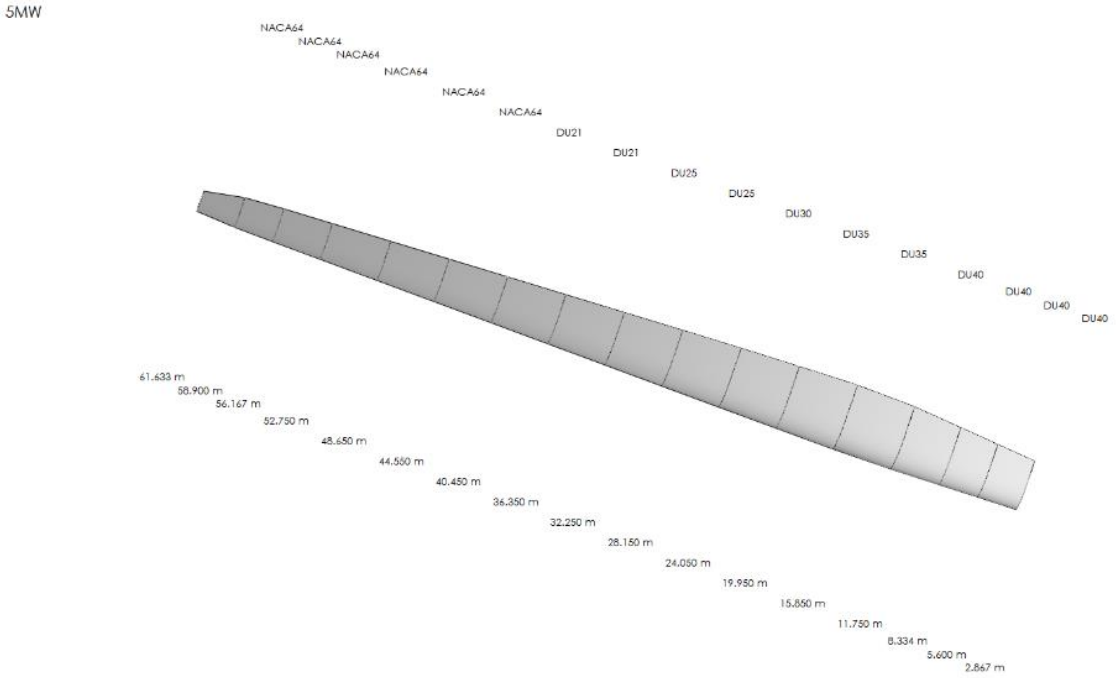

Figure 4: NREL 5MW Wind Turbine Blade with Adjusted Root Nodes 1-3

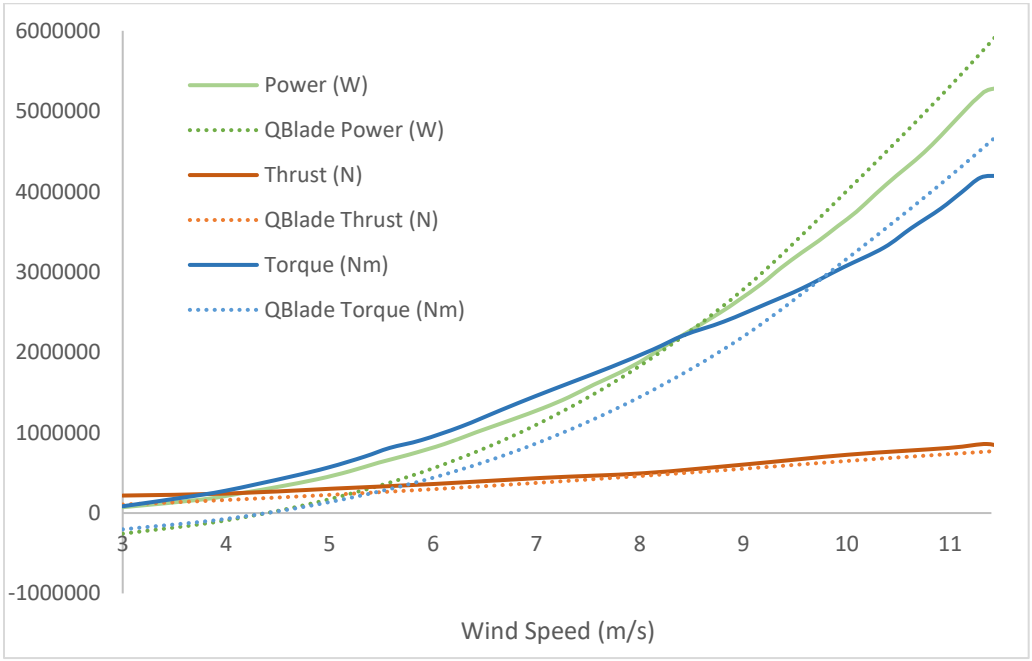

Figure 5: NREL 5MW Wind Turbine Outputs[7] ***and QBlade Rotor BEM Estimate Outputs vs Wind Speed***

With QBlade Rotor BEM data closely following the previously published FAST data, a simplified turbine blade, made up of NACA 0012 airfoils at an eight degree pitch angle, was explored at various tip speed ratios. Flow characteristics, blade geometry and operating conditions from the NREL turbine[7] were used in the following NACA 0012 case to provide consistency.

2.3.3 Conventional NACA 0012 Turbine

The NACA 0012 Turbine was also explored in StarCCM+ using two methodologies. One simulation consisted of a fully resolved blade in a 1/3 cut cylindrical domain with a rotating reference frame. The second used BEM in a stationary cylindrical domain. Geometry and boundary conditions of these domains can be seen in Figure 6 and Figure 8. To maintain accuracy of the results between the two methods, the fully resolved blade case required a significantly higher cell count compared to the BEM case. This is in part to capture the leading edge, trailing edge, and tip effects of the blade. The fully resolved, FR, case was computationally heavy with around thirty million cells[13], while the BEM case used about five-hundred thousand cells. Because of the differences in the mesh size, the number of iterations to convergence and CPU time per iteration were much larger in the FR case. Table 1 shows a comparison of properties between the two methods[14].

Table 1: Properties of NACA 0012 Turbine Computational Resources

	Fully Resolved Blade (FR)	Blade Element Method (BEM)
Cell Count	~ 30,000,000 Cells	~ 500,000 Cells
Iterations to Convergence	~ 3000 Iterations	~ 500 Iterations
CPU Solver Time per Iteration	~ 595 CPU Seconds	~ 27 CPU Seconds

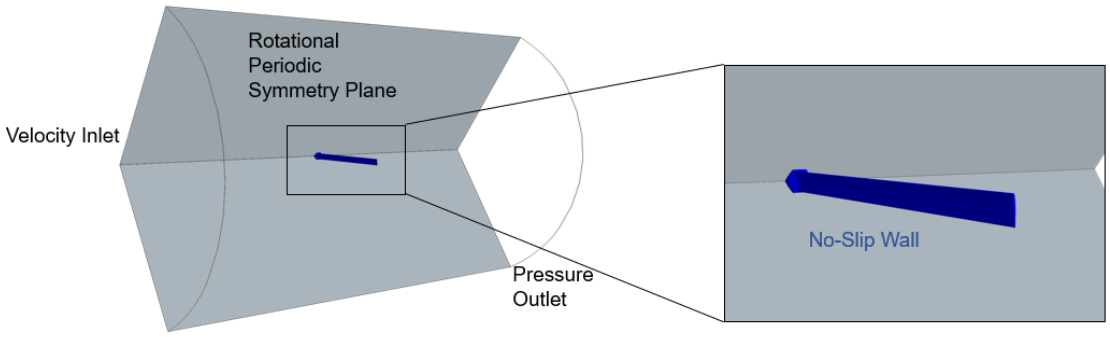

Figure 6: NACA 0012 Resolve Simulation – Domain Geometry

The two methods used require different amounts input data. The FR case requires airfoil coordinates and flow properties while BEM requires additional airfoil polar data as an input table. While QBlade uses an XFOIL derivative within its software to generate airfoil coordinates and aerodynamic data to be used downstream for its calculations, StarCCM+ requires these polar to be imported from an external source. To be consistent throughout the testing, the NACA 0012 aerodynamic information and coordinates generated by QBlade were used as input information for

the FR and BEM cases of the NACA 0012 Turbine. Airfoil aerodynamic data was generated with Reynold's numbers ranging from three-hundred thousand to 2.2 million corresponding with the expected range of the turbine.

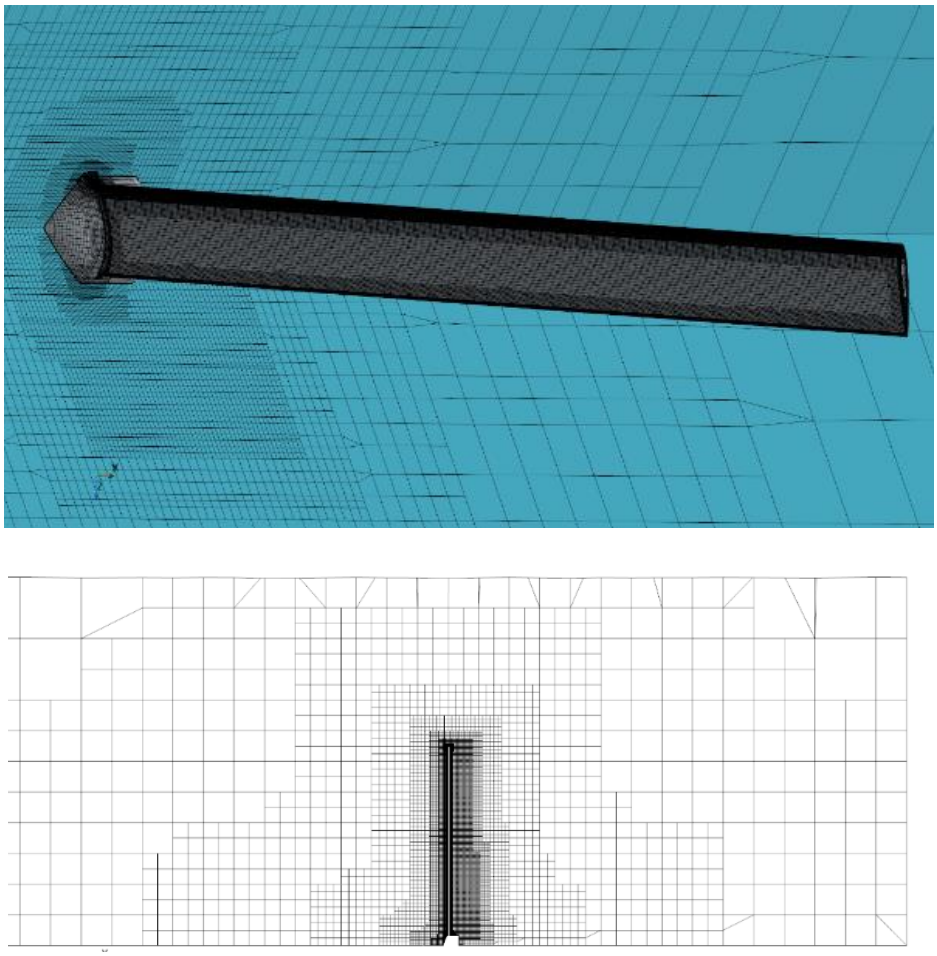

Figure 7: NACA 0012 Fully Resolved – Mesh

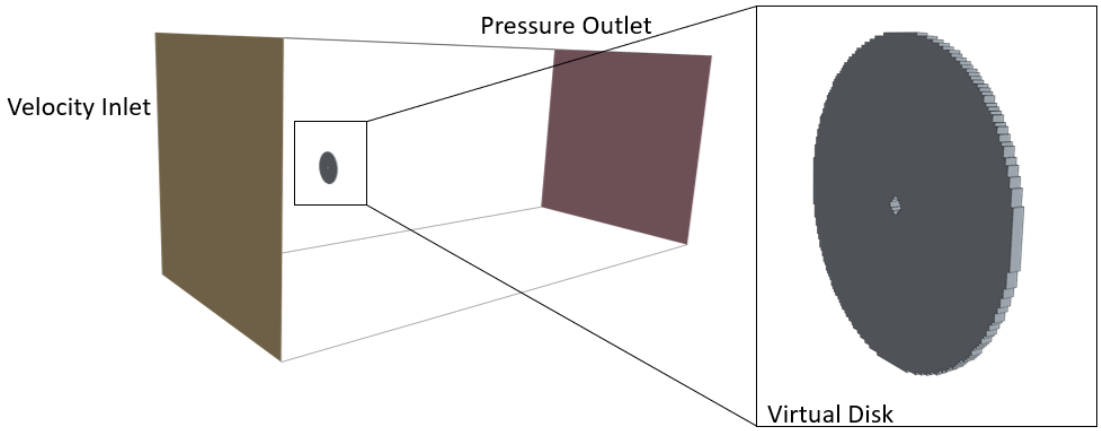

Figure 8: NACA 0012 BEM – Domain Geometry

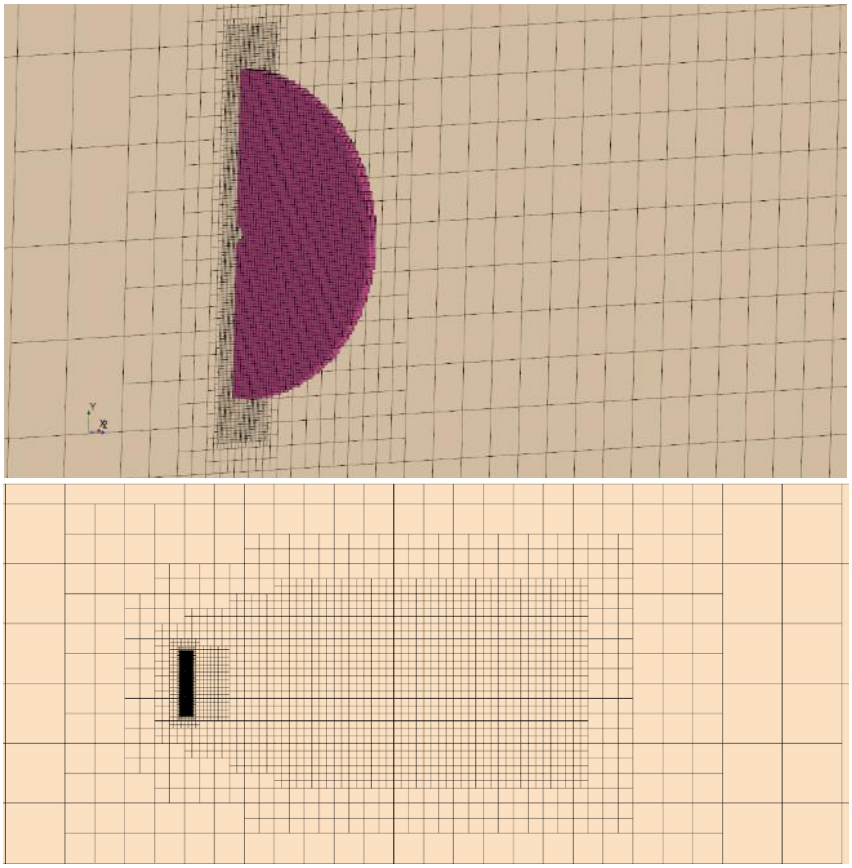

Figure 9: NACA 0012 BEM – Mesh

The results of the NACA 0012 turbine were explored using 4 different methods. Table 2 below contains power (C_p), torque (C_Q), and thrust (C_T) coefficients of the NACA 0012 Turbine at 11.4 m/s windspeed and 12.1 rpm for the 4 different cases. The results from QBlade, also referred to below as Potential Flow, are a power coefficient of 0.253, a torque coefficient of 0.0351, and a thrust coefficient of 0.361. While the theoretical results from Potential Flow for thrust are good, they overestimate the actual power and torque results of turbines at increasing wind speeds as shown in Figure 5 of the NREL 5MW wind turbine and expressed by Zhang [13]. For this reason, the BEM case was run using a constant tip loss correction factor initiated at 85% span. This case resulted in a power coefficient of 0.232, a torque coefficient of 0.0322, and a thrust coefficient of 0.337. Although unused in comparison plots below the results of a BEM case without tip loss correction can be found in Table 2. This case provided a power coefficient of 0.249, a torque coefficient of 0.0347, and a thrust coefficient of 0.355. The final case, the fully resolved case (FR), yielded a power coefficient of 0.222, a torque coefficient of 0.0308, and a thrust coefficient of 0.357. Power, torque, and thrust coefficients are defined as:

$$C_p = \frac{\Omega Q}{\frac{1}{2}\rho A v_\infty^3}$$

$$C_Q = \frac{Q}{\frac{1}{2}\rho A v_\infty^2 s}$$

$$C_T = \frac{T}{\frac{1}{2}\rho A v_\infty^2}$$

Since the potential flow case was validated against the previous FAST data with trends matching quite well aside from overpredictions on torque and power, the above cases were compared against it. Since torque and power were overpredicted by potential flow at operating condition of 12.1 rpm, cases that underpredicted these values compared to potential flow are beneficial. The BEM case without a tip loss correction factor delivered power and torque coefficients closest to the potential flow case with a 1.593% difference in power coefficient. This is expected as the two methods use the same input airfoil tables to calculate the lift and drag forces based on the localized inflow velocity and receive the least tip effects. This means that this case is likely also overestimating the power and torque of the turbine. The BEM case with a tip loss correction factor applied provided the second closest set of power and torque coefficients compared to potential flow. It underpredicted potential flow with an 8.66% difference in power coefficient which means this set of power and torque coefficient is likely closer to reality than potential flow. Finally, the fully resolved data was the furthest from potential flow with an underestimate of power coefficient at 13.05% difference. This makes it closest to the 24.29% difference below potential flow that FAST provided for the NREL 5MW blade.

Table 2: NACA 0012 – Coefficients Table at 12.1 RPM

	Power Coefficient	*Torque Coefficient*	*Thrust Coefficient*
BEM	0.232	0.0322	0.337
Fully Resolved	0.222	0.0308	0.357
Potential Flow (QBlade)	0.253	0.0351	0.361
BEM without Tip Loss Correction Factor	0.249	0.0347	0.355

While the potential flow solver, QBlade, overestimated torque and power compared to the previously published FAST data, its thrust results were quite close. Potential flow underestimated thrust by 3.87% difference compared to FAST. While none of the solver methods provided thrust values above what potential flow estimated for the NACA 0012 turbine, the fully resolved case was closest at 1.11% difference below the potential flow case. Closely behind this was the BEM without a tip loss correction at 1.68% difference and finally BEM with a tip loss correction at 6.88% difference.

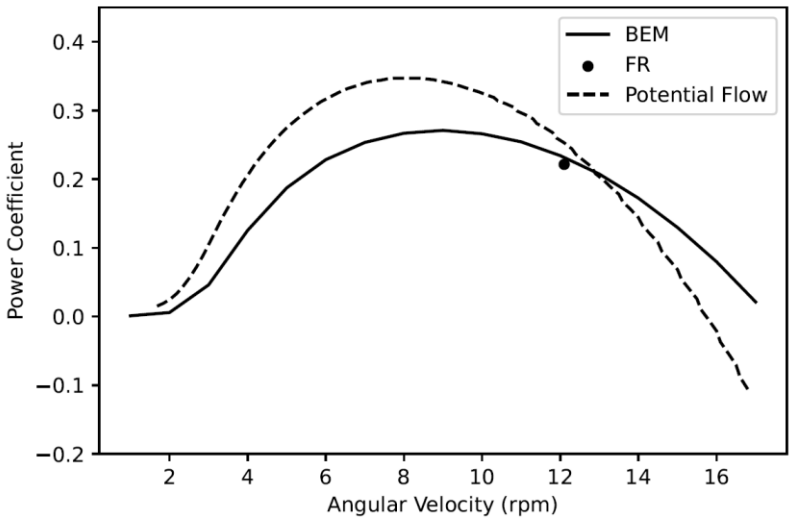

Figure 10: NACA 0012 – Power Coefficient Vs Angular Velocity at 11.4m/s Windspeed

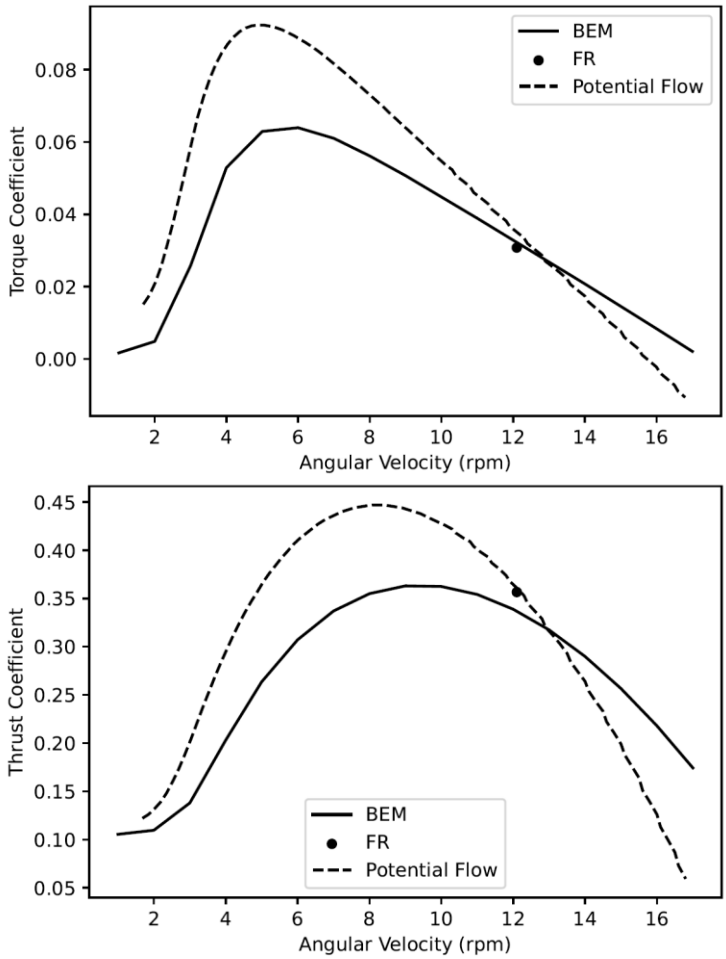

Figure 11: NACA 0012 – Torque Coefficient and Thrust Coefficient Vs Angular Velocity

Since potential flow greatly overestimated power and torque while slightly underestimating thrust, the results of the fully resolved case, which compared to potential flow, underestimate power and torque and slightly underestimates thrust, provide the most reasonable results. While the fully resolved case is likely the best result, the BEM results with a tip loss correction factor applied provide data within 6% difference of the fully resolved case. This is significant because as shown in Table 1, the BEM results were acquired with a mesh 60 times coarser and at a computation rate per iteration 22 times faster than the fully resolved case. This suggests that BEM using 2D aerodynamic data is a reasonable estimator for power, torque and thrust of the NACA 0012 turbine.

2.3.4 Sprayed Liquid Flap Equipped NACA 0012 Turbine

The NACA 0012 Turbine equipped with a Sprayed Liquid Flap was then explored in a fully resolved case and a BEM with tip loss correction. The SLF was implemented at the site 8 location on the pressure side of the blade. This location was chosen due to the significant changes in aerodynamic performance as indicated by models created by Loubimov [4]. Figure 12 shows the location of the dispersal site on the blade in 2D and 3D. Aerodynamic tables for the SLF equipped NACA 0012 airfoil were a requirement for the BEM cases. These tables were acquired by extending the Reynold's Number and angle of attack ranges on Loubimov's 2D SLF equipped NACA 0012 study [4,5].

The domain geometry, flow conditions, and boundary conditions were held constant between the NACA 0012 Turbine and the SLF equipped NACA 0012 Turbine (SLF Turbine) for both the fully resolved and BEM cases. Contrary to this, the mesh for the fully resolved case of the SLF Turbine, however, did require a change. To better capture the euler-euler droplet effects, the volume mesh resolution was refined within a region surrounding the blade. The refined region can be viewed in Figure 11. Due to the increase in grid resolution and the implementation of multiphase physics, the computational cost of the fully resolved case for the SLF Turbine was significantly greater than its NACA 0012 Turbine counterpart.

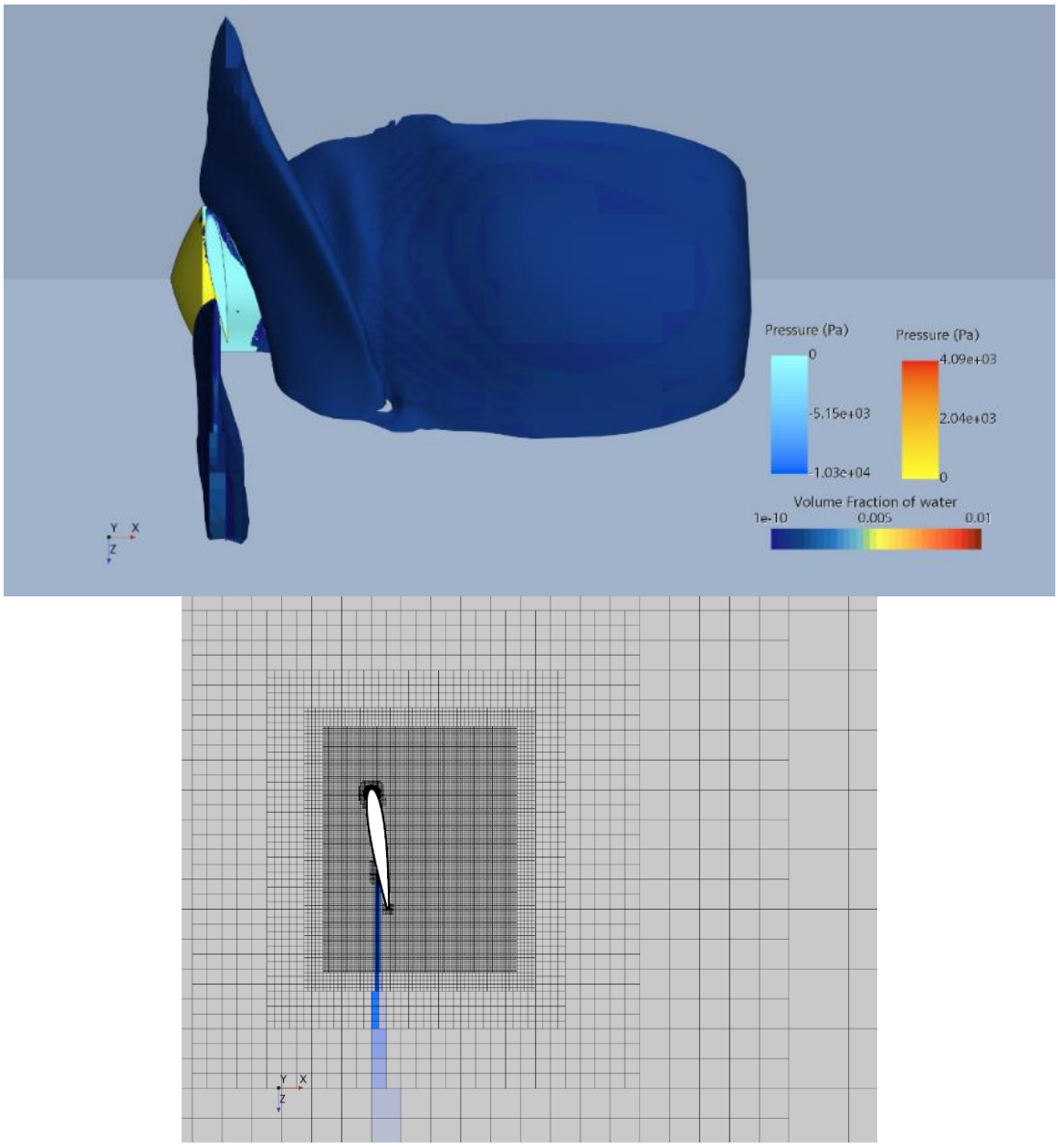

Figure 12: SLF NACA 0012 Fully Resolved – Steady Spray and Dispersal Site

Table 3 displays properties of the computational resources for the SLF Turbine. The cell count of the fully resolved SLF Turbine case (SLF FR) is close to 50 million cells and the CPU solver time per iteration was close to 1970 CPU seconds. This results in a sizeable increase from

the NACA 0012 Turbine's fully resolved case which used around 30 million cells and 595 CPU seconds per iteration. Opposing the increase of computation time for the SLF FR case caused by mesh refinement and multiphase effects, the computational properties of the SLF BEM case were unchanged from their BEM counterpart and thus the computation time is equivalent to that of the NACA 0012 Turbine's BEM case. This highlights the opportunity to explore multiphase rotating flows for cheap.

Table 3: Properties of SLF Equipped NACA 0012 Turbine - Computational Resources

	Fully Resolved Blade (SLF FR)	*Blade Element Method (SLF BEM)*
Cell Count	~ 50,000,000 Cells	~ 500,000 Cells
Iterations to Convergence	~ 2500 Iterations	~ 500 Iterations
CPU Solver Time per Iteration	~ 1970 CPU Seconds	~ 27 CPU Seconds

While the blade element method is cheap, it lacks the ability to determine blade surface pressures like a fully resolved blade simulation does. The fully resolved blade cases calculated these surface pressures and their respective plots of pressure coefficient versus normalized chord position (x/c) at varying spanwise locations can be seen in Figure 13. Since the SLF was equipped at site 8 of the NACA 0012 airfoil, which corresponds with 75% chord, designated by Loubimov,

a spike in negative pressure was seen at 0.75 x/c at all spanwise positions on the pressure side of the blade [3]. This spike is due to the additional momentum from the liquid spray interrupting the typical flow and asserting flap like effects to the airfoil. Since the spray was pushing outward from the surface of the blade, the pressure on the blade was negative at and past the ejection site. While decreased pressure on the pressure side of an airfoil typically relates to a decrease in lift coefficient, since the sprayed liquid flap provides effects like a mechanical flap without geometric changes to the airfoil, the camber of the airfoil is effectively changed, and pressure on the surface of the airfoil at and past the SLF region is no longer a good indicator of changes to lift coefficient since the effective and geometric cambers no longer match. Figure 14 compares the lift coefficient versus spanwise position along the blade for the BEM, SLF BEM, and potential flow cases including no tip loss correction. While the BEM and potential flow cases follow similar trends, the SLF BEM case provided a significantly higher lift after 0.25 r/R. Since increased lift leads to increased torque and thereby increased power, maximizing the increase of lift provided by the SLF should theoretically lead to maximal power gains. With this in mind, as spanwise position increased, the additional lift created by the SLF also increased. Since the SLF BEM case used 2D airfoil polars that were created using a constant jet velocity, it can be said that the lift benefits of the SLF are dependent on a combination of the jet velocity and wind inflow.

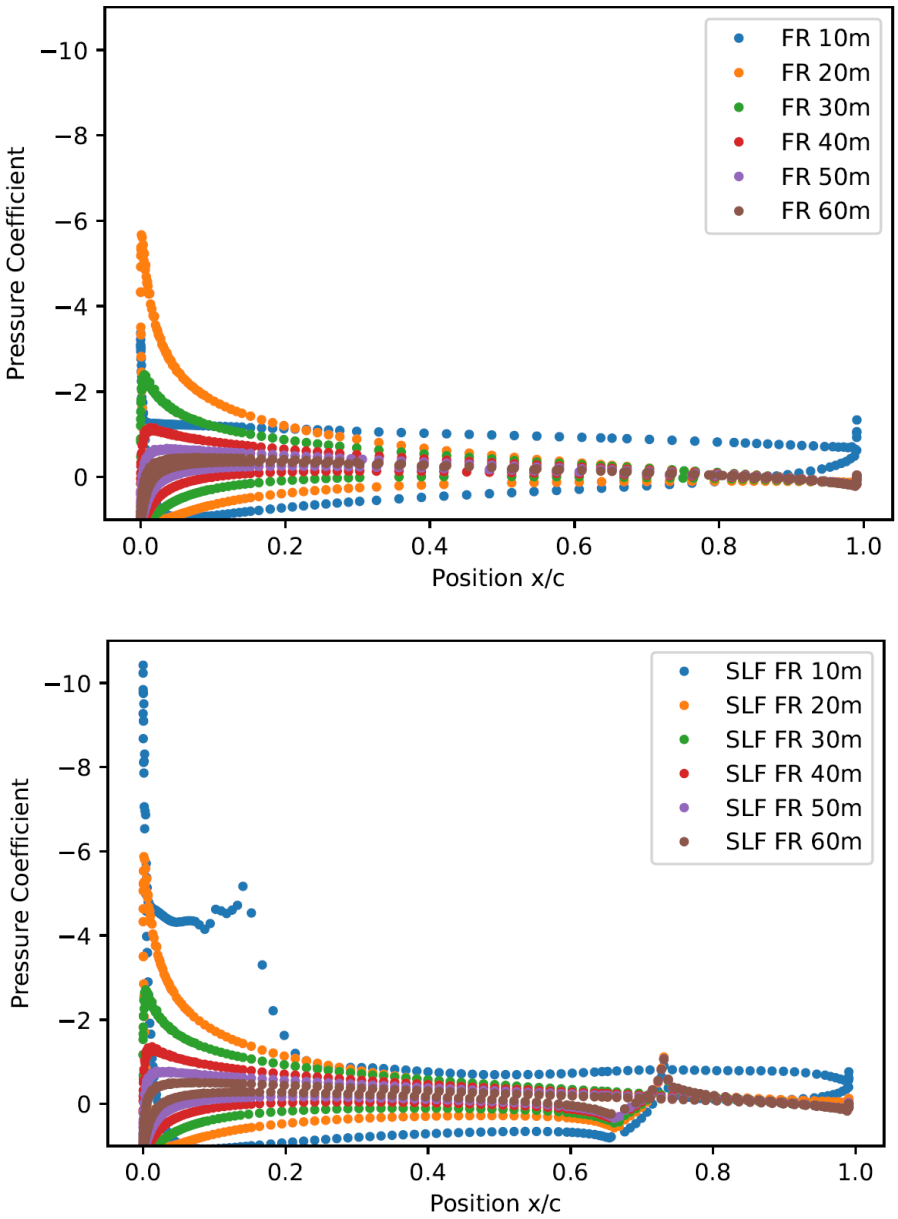

Figure 13: NACA 0012 and SLF NACA 0012 – Pressure Coefficient Vs Chord at Varying Span Positions

The lift benefits of the SLF are not prevalent at all combinations of jet velocity and wind inflow. Figure 14 shows a reduction in lift for the SLF BEM case at spanwise positions along the

blade less than 0.25 r/R. While there is likely to be an optimal combination of factors for each airfoil, in a large-scale rotational system where the inflow condition changes drastically along the radius of the blade, a constant jet velocity will provide undesirable effects at some locations. The SLF NACA 0012 Turbine has a 61.5m blade and a 3.25m hub leading to large differences in inflow speed along the blades during rotation. In Figure 17 power coefficient of the conventional and SLF equipped turbines are compared. At higher angular velocities the power benefits of the SLF can be seen, but at lower rates the SLF negatively affects the lift coefficient and thus power reductions can be seen. Since the rated speed of the NREL turbine was 12.1 rpm, the rated speed of the SLF NACA 0012 Turbine is assumed to be similar. Under this condition, the SLF implementation provides a large boost to power generation.

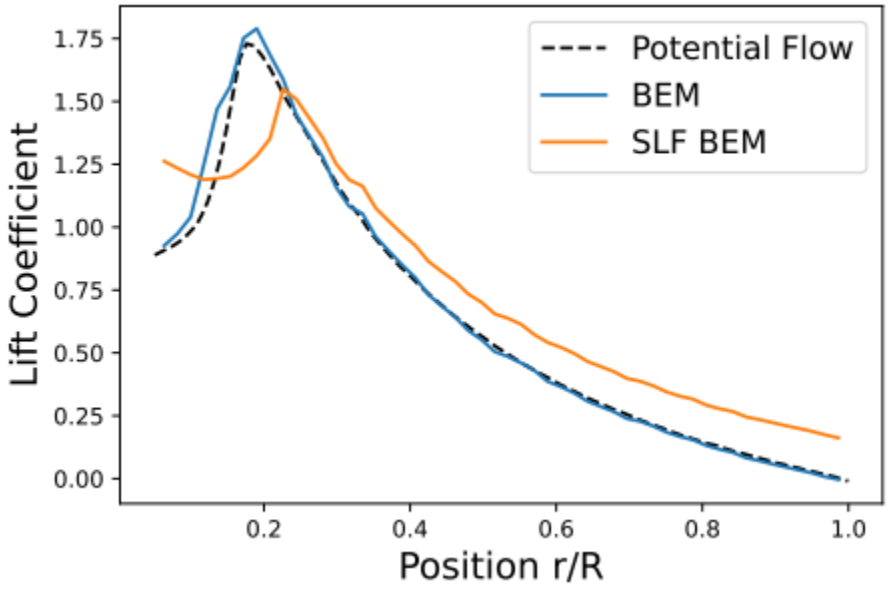

Figure 14: NACA 0012 and SLF NACA 0012 – Lift Coefficient Vs Position r/R Along One Turbine Blade

At the assumed operating condition of 12.1 rpm, the SLF Turbine provided increases to power, torque, and thrust compared to the conventional turbine. This was true for both the fully resolved SLF case (SLF FR) and the SLF BEM case. Table 4 holds the values of power, torque, and thrust coefficients for both SLF cases.

Table 4: SLF NACA 0012 – Coefficients Table at 12.1 RPM

	Power Coefficient	*Torque Coefficient*	*Thrust Coefficient*
SLF BEM	0.303	0.0422	0.441
SLF FR	0.289	0.0401	0.469

With the activation of the sprayed liquid flap, the power coefficient of the SLF FR case was 0.067 greater than the conventional fully resolved case. Similarly, the SLF BEM power coefficient was 0.071 greater than the BEM case. As previously discussed about the conventional NACA 0012 Turbine, the fully resolved case provided the most reasonable results and should be taken as the expected results. The SLF FR case provided a power coefficient of 0.289, a torque coefficient of 0.0401, and a thrust coefficient of 0.469. Compared to the SLF FR case, SLF BEM once again overestimated power and torque while underestimating thrust. The SLF BEM case provided 0.303 for power coefficient, 0.0422 for torque coefficient, and 0.441 for thrust coefficient. This yields a 4.84% difference in power, 5.24% difference in torque, and a 5.97% difference in thrust. With blade element data once again falling within 6% difference of the fully resolved data, SLF BEM

sweeps of angular velocity were run to preliminarily explore conditions other than the rated speed. Figure 15 and Figure 16 show the SLF BEM sweeps of power then torque and thrust coefficient versus angular velocity at the same rated wind speed of 11.4 m/s. The SLF BEM data shown was run with the inclusion of a constant tip loss correction factor applied at a radial starting point of 0.85 r/R as previously done for the NACA 0012 Turbine case.

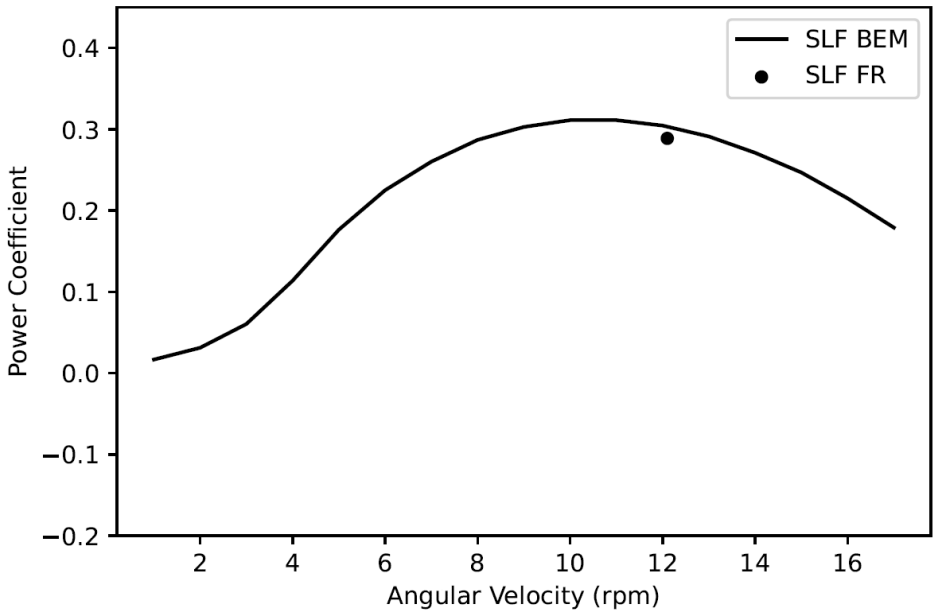

Figure 15: SLF NACA 0012 – Power Coefficient Vs Angular Velocity at 11.4m/s Windspeed

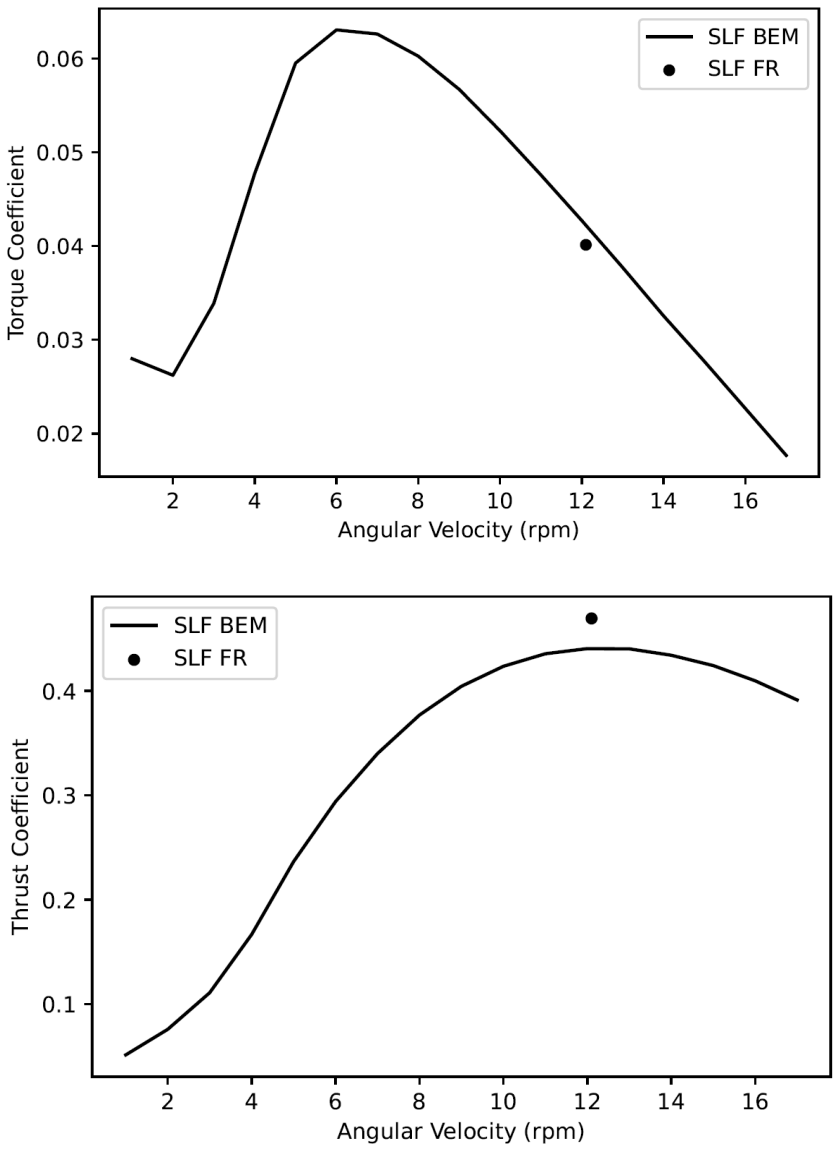

Figure 16: SLF NACA 0012 – Torque and Thrust Coefficient Vs Angular Velocity

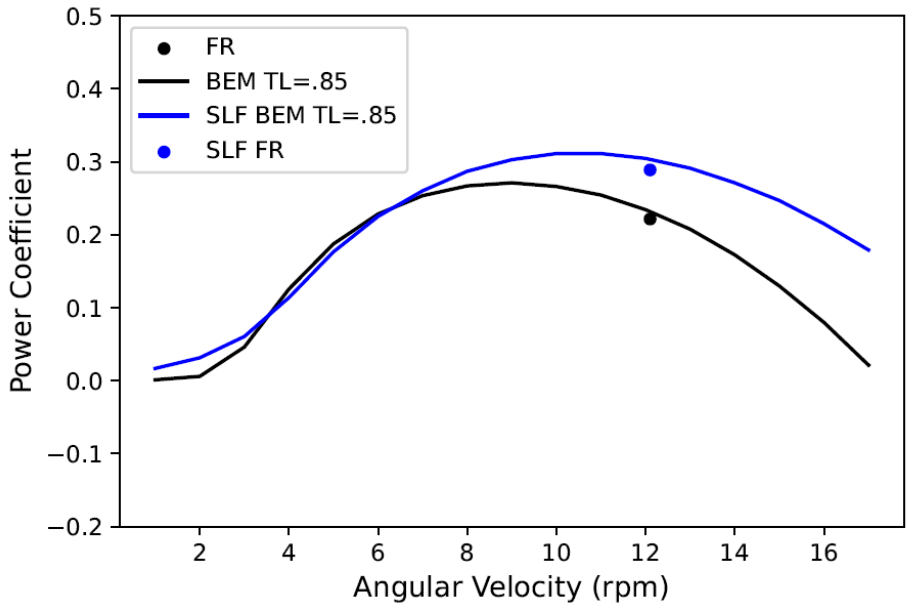

Figure 17: NACA 0012 and SLF NACA 0012 – Comparison of Power Coefficient vs Angular Velocity

2.4 Conclusion

The effects of a Sprayed Liquid Flap applied to a wind turbine equipped with a NACA 0012 blade with the dimension of a NREL 5MW turbine were investigated. Published data for the NREL 5 MW turbine was compared with the potential flow solver QBlade to validate the solver's ability to model turbine output characteristics. From there, two methods of modeling turbines in the CFD software StarCCM+, a fully resolved blade and Blade Element Momentum Method, were validated against potential flow. The results of both a NACA 0012 turbine and a SLF equipped NACA 0012 turbine were compared using BEM and fully resolved methods. Both methods showed that the SLF equipped turbine produced higher power, torque, and thrust coefficients than the NACA 0012 turbine at the assumed rated operating condition.

The results of BEM were compared against the potential flow data and the fully resolved blade data to determine its effectiveness to model turbine characteristics from 2D airfoil aerodynamics. BEM provided well placed estimates at the explored condition with significant reductions to computational load when compared to the fully resolved blade cases for the NACA 0012 case. It then continued to provide good estimates and higher reductions in computation time for the SLF equipped turbine.

From this study alone, conclusions cannot be made on the effectiveness of BEM as an estimator for SLF equipped turbines due to the amount of fully resolved data used, but the initial results show one example where BEM estimates 3D multiphase physics using 2D SLF airfoil aerodynamic data. Once this has been validated more, SLF's potential as solutions to issues such as restricted power generation envelopes, overbuilt structural components, and backup brake methods could be explored with fewer computational resources.

CHAPTER 3: TIP LOSS CORRECTION FOR A SPRAYED LIQUID FLAP EQUIPPED TURBINE

3.1 Introduction

The previous study on the sprayed liquid flap equipped NACA 0012 wind turbine explored the benefits of BEM as an estimator for multiphase rotational flow but fell short of drawing conclusions due to a limitation of fully resolved data for the SLF Turbine to compare against. Expanding upon the fully resolved data provides the opportunity to validate the Blade Element Momentum Method's estimation ability across a range of rotation rates. This would provide a pathway to future research into the rotational applications of the sprayed liquid flap for cheap. Thus, in this study the fully resolved data for the SLF Turbine will be expanded over a range of rotation rates.

Expanded fully resolved data allows for more in-depth comparisons to be made between the BEM and FR cases and help showcase any inaccuracies within the BEM estimates. These differences will be discussed, and possible solutions will be proposed. Tip loss correction, one such tunable solution, will be explored and a study comparing two different methods of tip loss correction will be compared.

3.2 Methods

3.2.1 Tip Loss Correction Factor

The Blade Element Momentum Method converts lift and drag coefficients as functions of Reynolds number and angle of attack to a set of forces at discretized sections along a blades span. This is done using the equations listed in section 2.2.3 Blade Element Momentum Method. This approach is inviscid and assumes there are no interactions between blade segments which leads to the methods inability to capture any 3-dimensional effects on the blade. One such effect is the recirculation effects of the tip vortices which reduces the near tip blade sections effective angle of attack [15,16]. These reduction effects can be modeled through the inclusion of a tip loss correction factor. During calculations of the lift and drag, the forces at specified blade segments are multiplied by this tip loss correction factor to account for the reduction of effective angle of attack. This factor ranges from 0 to 1 and in StarCCM+, the tip loss correction factor is applied at a specified radial starting location which is a value of r/R or normalized radial span position [8].

There are numerous tip loss correction factor methods that can be applied to BEM to accurately capture the tip effects. Some common of these methods include constant, cosine, and Prandtl tip loss. Constant tip loss correction uses a step function with a value of 1 up until its radial starting location then a factor of 0 after it. This essentially negates the effects of calculated forces. Instead of a hard drop of forces, the cosine tip loss uses a piecewise half-cosine wave function to gradually reduce the influence of the forces on segments after its radial location. The equation StarCCM+ uses for its cosine tip loss correction factor is:

$$F = \begin{cases} 1, & 0 \le r' < r'_{start} \\ \cos\left[\frac{\pi}{2}\left(\frac{r' - r'_{start}}{R - r'_{start}}\right)\right], & r'_{start} \le r' \le R \end{cases}$$

One other such method of tip loss correction was proposed by Prandtl and has since been given multiple variations by Glauert and more recently Burton [17,18]. The Prandtl tip loss correction factor is a function of three radial variables, an axial induction factor, and an angular induction factor. Differing the assumptions that limit the above variables provide the variations proposed by Glauert and Burton. Equations for Prandtl tip loss and its variations are:

$$F_{Prandtl} = \frac{2}{\pi}\arccos\left[\exp\left(-\frac{N_b(R - r_1)(\sqrt{(V_n^2 + V_t^2)}}{2r_2 V_n}\right)\right]$$

$$F_{Glauert} = \frac{2}{\pi}\arccos\left[\exp\left(-\frac{N_b(R - r)}{2r sin\phi(r)}\right)\right]$$

$$F_{Burton} = \frac{2}{\pi}\arccos\left[\exp\left(-\frac{N_b(R - r)}{2r}\sqrt{1 + \left(\frac{\lambda(r)}{1 - a(r)}\right)^2}\right)\right]$$

As suggested by Ramdin [2], simple assumptions like aligning radial position variables with either the local position or the tip position led to numerous possible variations. This drives the need for tuning of the tip loss correction factor based on previously validated data. While StarCCM+ does not have a direct implementation of the Prandtl tip loss correction factor, it does have a user defined function tip loss correction factor setting which can be used to correct either lift, angle of attack, or lift and drag together based on the radial starting point and inflow conditions. This method of implementing a more robust tip loss correction factor like Prandtl's tip loss will be explored in future works.

3.3 Results

3.3.1 Extended Fully Resolved SLF NACA 0012 Turbine Data

In hopes of further suggesting the validity of BEM as an estimator for rotational multiphase physics, the range of fully resolved data on the SLF Turbine was extended across angular velocities ranging from 4 to 16 revolutions per minute. Figure 18 shows power coefficient versus angular velocity of the extended data coplotted against two SLF BEM cases with constant tip loss correction factor applied at different radial starting positions. The dotted line is representative of the BEM case with no tip loss correction factor applied as its normalized radial starting position is 1. The solid line is BEM with a constant correction factor applied at 0.85 normalized radial position. The constant tip loss corrected data does a decent job at estimating the fully resolved data up until the rated operating speed of 12.1 rpm before losing the trend. The no tip loss case seems to better match the trend of the curve, especially in the upper range of angular velocities when compared to the 0.85 constant tip loss case, but overestimated power along the entire range of data.

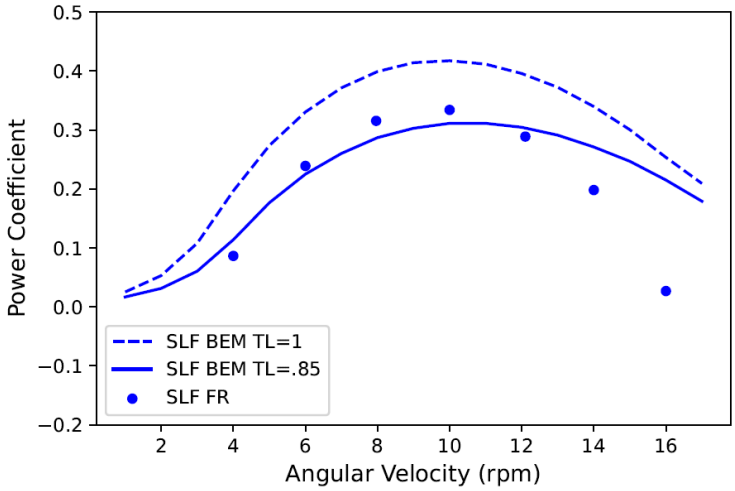

Figure 18: SLF NACA 0012 – Extended Fully Resolved Data of Power Coefficient Vs Angular Velocity

Since BEM has proven to be quite and effective estimator for turbulent rotational physics despite its inviscid nature, the error in its estimations here are expected to be due to one of two things: 1) lack of proper tuning of the tip loss correction factor or 2) error in the 2D SLF equipped NACA 0012 polars used by BEM. Some of the largest errors of BEM estimations come from the tip effects, and the input polar data [15]. As suggested by Schneider, polar data extracted from 3D CFD simulations will greatly increase the accuracy of BEM estimations [19]. The polars used for the SLF NACA 0012 Turbine were created using 2D CFD within the linear lift versus angle of attack range and did not include any values at or post stall. With a constant twist distribution turbine like the SLF Turbine, there are sections of the blade that are exposed to post stall angles of attack which will likely cause error due to the lack of data outside the linear region. Because of the computational cost associated with generating 3D unsteady multiphase CFD polars for the SLF NACA 0012 airfoil post stall, adjusting the input polar is outside the scope of this paper but future works would include recalculations of the input polars using 3D CFD. Instead, initial tuning of the tip loss correction factor was explored to determine the functionality of StarCCM+'s constant and cosine tip loss correction factors for this turbine.

3.3.2 Tip Loss Correction Factor Study

The implementations of constant and cosine tip loss correction factors are determined by a normalized radial starting position (r/R). Tuning this variable alters the shape of the resultant BEM curve allowing for better estimates of desired effects. Figure 19 shows a combination of BEM power coefficient curves with different constant and cosine tip loss correction factors coplotted

with the extended fully resolved data for the SLF NACA 0012 Turbine. Both correction methods were explored at a range of normalized radial starting positions from 0.7 to 1 at a 0.05 increment. Constant tip loss immediately disregards the forces produced after its activation and thus has a much larger adjustment to the power curve than cosine tip loss which at activation gradually decreases its factor value to zero. Within Figure 19 constant correction is shown with constant lines and cosine correction is shown with dashed lines. The cosine correction factor consistently overestimated the expected power coefficient within the range of starting locations. While the power coefficient at lower rotation rates using cosine tip loss show meaningful adjustment at each increment of starting position, at the higher angular velocities the effects of cosine tip loss correction are less pronounced. That means unless the uncorrected BEM results are very close to the desired values at higher turbine rotation rates, cosine tip loss correction may not correct the BEM result enough to provide good estimates at these conditions. Because the uncorrected BEM power curve overestimated the fully resolve data at all rotation rates, shown in Figure 18, cosine tip loss correction factor was not the best method of estimating tip effects.

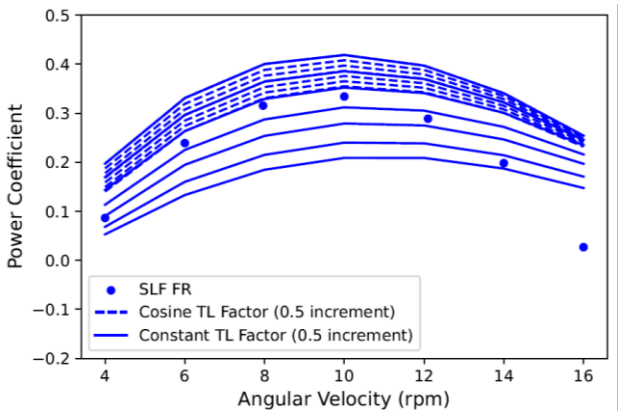

Figure 19: SLF NACA 0012 – Tip Loss Correction Factor Radial Starting Point Study

Constant tip loss correction provided larger changes to the BEM power curve than cosine tip loss which in this case, where the uncorrected BEM results overestimate the SLF FR power coefficient, proves to provide better estimates within the explored conditions. Figure 20 and Figure 21 are parity plots of the tip loss correction data plotted in Figure 19 with cosine data in the first plot and constant data in the second. The cosine method has data inside a 15% estimation range at only 3 rotation rates while the constant method has data within the estimation range at 6 of the 7 rotation rates. Of the constant tip loss correction radial starting positions, the 0.85 value provided the most data points within the estimation range. It was inside the range at 4 rotation rates and was close to inside the range at 2 rates. This finding supports the SLF BEM data found in the previous section, 2.3.4 Sprayed Liquid Flap Equipped NACA 0012 Turbine, which looked at the differences of SLF BEM with a constant tip loss correction factor implemented at 0.85 r/R compared to fully resolved data and potential flow.

The fully resolved power coefficient at 16 rpm was the only location where neither cosine nor constant tip loss correction were able to estimate the fully resolved point within the 15% estimation range. The uncorrected BEM result at 16 rpm was too overestimated for tip loss correction factors to be effective. This leads back to the largest potential factors of error in BEM, one of which is accuracy of the aerodynamic input polars. With the results of the tip loss correction study providing estimates significantly higher than fully resolved data in the upper range of rotation rates, it could be inferred that the 2D CFD input polar are not accurately capturing lift and drag coefficients at those inflow conditions. With that working assumption, a set of 3D CFD input polars with an extended range angle of attack range into the stall region would provide better estimates for BEM of SLF equipped turbines.

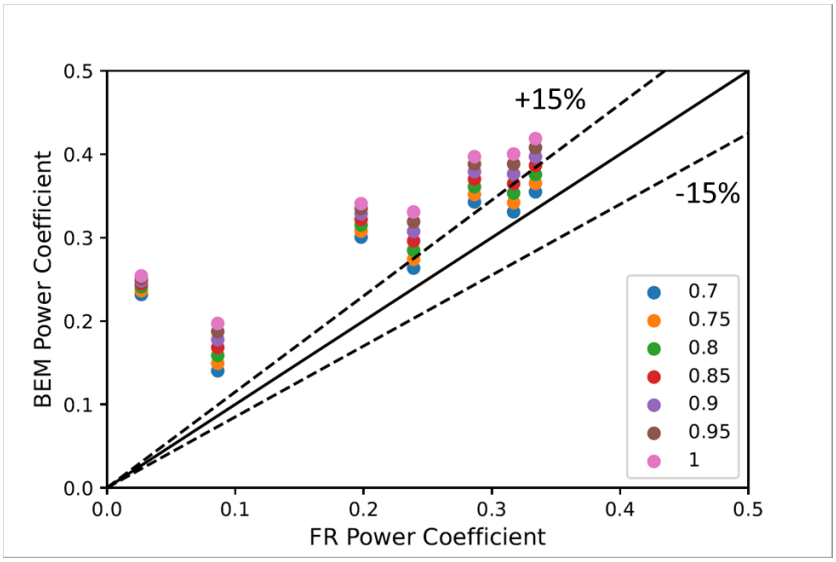

Figure 20: Parity Plot of BEM and FR Power Coefficient – Cosine Tip Loss Correction at Varying Normalized Radial Starting Position (r/R)

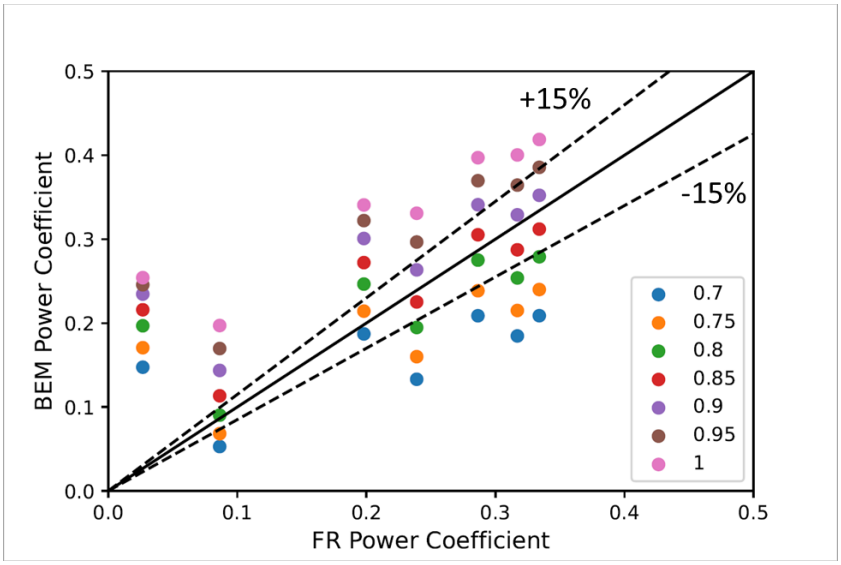

Figure 21: Parity Plot of BEM and FR Power Coefficient – Cosine Tip Loss Correction at Varying Normalized Radial Starting Position (r/R)

3.4 Conclusion

The Blade Element Momentum Method provides a potential avenue to research rotational multiphase flows as a tunable, cost-effective estimation tool. The fully resolved SLF NACA 0012 Turbine was explored across a range of rotation rates and compared to previously calculated SLF BEM curves using 2D multiphase aerodynamic polars. The comparison showed significant differences in power coefficient curve shapes between the two methods especially at rotation rates above the rated operating rate. Two potential sources of error were discussed and one source, tuning of the tip loss correction factor, was addressed in an exploration study. The study yielded results suggesting the already used constant tip loss correction factor initiated at 0.85 r/R was the ideal solution for estimating power coefficient along the entire range of rotation rates explored, however, other robust tip loss correction methods like Prandtl tip loss could provide better solutions but require tools external to StarCCM+. One fully resolved power coefficient value was not reached by either tip loss correction method used in the study. The power coefficient at the fastest rotation rate of 16 rpm was overestimated in all BEM sweeps run. This occurrence highlights the need to explore the aerodynamic input polars as the second source of error in the BEM estimates. The limitations of the 2D, pre-stall, airfoil tables have likely been reached and if exploration at higher rotation rates is desired, moving to 3D, early stall inclusive airfoil tables should increase the accuracy of the BEM estimates.

CHAPTER 4: CONCLUSION

4.1 Conclusion

This thesis aimed to investigate the performance of a SLF equipped wind turbine and assess the effectiveness of the BEM as a cheap avenue for researching rotational multiphase flows. The findings of this thesis provide insights into the benefits of the SLF as a power generating technology for wind turbines and methods of tuning BEM for SLF equipped wind turbines.

In Chapter 2, the effects of a SLF NACA 0012 wind turbine were compared to a conventional NACA 0012 turbine. Through validation of the potential flow solver QBlade against previously published data of the NREL 5MW turbine and the comparison of potential flow, BEM, and fully resolved blade cases, it was observed that the SLF turbine provided higher power, torque, and thrust coefficients compared to the conventional turbine at the assumed rated operating condition. Furthermore, BEM's ability to estimate 3D multiphase physics using 2D SLF airfoil aerodynamic data was showcased, although more validation was necessary to make conclusions.

In hopes of providing more evidence for BEM as an estimator for rotation multiphase flows, the third chapter expanded on the fully resolved data for the SLF NACA 0012 turbine and compared it with the previously generated SLF BEM power coefficient curves across a range of rotation rates. The comparison revealed differences in power coefficient values along the rotation range, especially at rotation rates above the rated operating condition. One potential source of estimation error for the BEM results, tip loss correction, was addressed in a study and it was found that the already used method of constant tip loss applied at 0.85 r/R was the ideal solution for the current scenario. With tip loss correction accounted for, the overestimation of power coefficient at

the upper range of rotation rates could be due to the limitations of the 2D, pre-stall, airfoil input tables used by BEM. Moving to 3D, early stall inclusive, airfoil input tables was suggested to improve BEM estimations, particularly at higher rotation rates.

In conclusion, the performance of a SLF equipped wind turbine and the potential of BEM as an estimator for rotational multiphase flows were explored. The results add to current efforts to improve wind turbine power generating technologies and provide a pathway for cheap future research.

4.2 Future Works

The subsections below aim to introduce or reiterate presentable future research for a SLF equipped wind turbine.

4.2.1 Tip Loss Correction Factor

The current works of this thesis scratch the surface of the tip loss correction methods available. Constant and cosine tip loss correction factors are easily accessible within StarCCM+ but more robust corrections, such as variations of the Prandtl tip loss correction, were spoken of and their potential for improvement of SLF BEM results is probable due to their extensive validation history on conventional turbines and propellers [2,17–20]. That being said, tip loss correction factor is only one form of estimation tuning and the aforementioned aerodynamic input polars fed to BEM can provide larger changes to its estimates.

4.2.2 Three Dimensional CFD Polars for the SLF NACA 0012 Airfoil

As highlighted in 3.3.2 Tip Loss Correction Factor Study, the constant tip loss correction factor applied at a radial location of 0.85 r/R was determined to best estimate the fully resolved results of the SLF Turbine. This was assuming the use of the specific 2D aerodynamic input tables. As suggest by Schneider [19], the estimations of BEM using 3D polar data are notably more accurate. Since generating 3D polars is more computationally expensive, a middle ground of 2D polars over an extended angle of attack range which can be interpolated over 360 degrees would likely provide better estimates than the current 2D polars while not drastically increasing computational cost.

4.2.3 SLF Braking

As shown in 2.3.4 Sprayed Liquid Flap Equipped NACA 0012 Turbine, the use of a sprayed liquid flap on the pressure side of wind turbine blade can produce additional torque at a designed operation condition through increases to lift. Similarly, if applied to the suction side of the blade, the SLF can provide a decrease in lift along the blade resulting in a decrease in torque. This addressable torque reduction could provide a new method of braking that could be beneficial for gust alleviation.

REFERENCES

[1] Wiser, R., Bolinger, M., Hoen, B., Millstein, D., Rand, J., Barbose, G., Darghouth, N., Gorman, W., Jeong, S., and Paulos, B. *Land-Based Wind Market Report: 2022 Edition*. 2021.

[2] Ramdin, S. F. *Prandtl Tip Loss Factor Assessed*.

[3] Loubimov, G. E., Fontes, D. H., and Kinzel, M. P. Three Dimensional CFD Analysis of the Sprayed Liquid Flap. 2022.

[4] Loubimov, G., Fontes, D., Loving, G., and Kinzel, M. Using Liquid Spray Formations to Improve Aerodynamic Performance of Airfoils. 2020.

[5] Spitzer, A., Loubimov, G. E., and Kinzel, M. P. An Evaluation of a Sprayed Liquid Flap on a 3D Wind Turbine Blade. 2023.

[6] Johnson, S. J., Baker, J. P., Van Dam, C. P., and Berg, D. "An Overview of Active Load Control Techniques for Wind Turbines with an Emphasis on Microtabs." *Wind Energy*, Vol. 13, Nos. 2–3, 2010, pp. 239–253. https://doi.org/10.1002/we.356.

[7] Jonkman, J., Butterfield, S., Musial, W., and Scott, G. *Definition of a 5-MW Reference Wind Turbine for Offshore System Development*. 2009.

[8] Siemens. Star-CCM+ User's Manual.

[9] Vieira, B. A., Kinzel, M. P., and Maughmer, M. D. CFD Hover Predictions Including Boundary-Layer Transition. 2017.

[10] Belayneh, M., and Ayalew, A. “DESIGN AND MANUFACTURING OF DIRECT DRIVEN STANDALONE WIND ENERGY CONVERSION SYSTEM.” 2013. https://doi.org/10.13140/RG.2.1.1031.4404.

[11] Samuell, M. *Computational Fluid Dynamic Modeling and Analysis of Small Scale Horizontal Axis Wind Turbines Recommended Citation*. 2017.

[12] Hermann Föttinger Institute of TU Berlin. QBlade.

[13] Zhang, Y., and Kim, B. “A Fully Coupled Computational Fluid Dynamics Method for Analysis of Semi-Submersible Floating Offshorewind Turbines Underwind-Wave Excitation Conditions Based on OC5 Data.” *Applied Sciences (Switzerland)*, Vol. 8, No. 11, 2018. https://doi.org/10.3390/app8112314.

[14] Cornelius, J. K., Schmitz, S., and Kinzel, M. P. “Efficient Computational Fluid Dynamics Approach for Coaxial Rotor Simulations in Hover.” *Journal of Aircraft*, Vol. 58, No. 1, 2021, pp. 197–202. https://doi.org/10.2514/1.C036037.

[15] Bangga, G. “Comparison of Blade Element Method and CFD Simulations of a 10 MW Wind Turbine.” *Fluids*, Vol. 3, No. 4, 2018. https://doi.org/10.3390/fluids3040073.

[16] Ingram, G. *Wind Turbine Blade Analysis Using the Blade Element Momentum Method. Version 1.1*. 2011.

[17] Prandtl, L., Betz, A., Klassiker der Strömungsmechanik, G., and Abhandlungen, V. Universitätsverlag Göttingen Universitätsverlag Göttingen Vier Abhandlungen Zur Hydrodynamik Und Aerodynamik.

[18] Glauert, H. Airplane Propellers. In *Aerodynamic Theory*, Springer Berlin Heidelberg, Berlin, Heidelberg, 1935, pp. 169–360.

[19] Schneider, M. S., Nitzsche, J., and Hennings, H. Accurate Load Prediction by BEM with Airfoil Data from 3D RANS Simulations. No. 753, 2016.

[20] Hansen, M. O. L., and Johansen, J. Tip Studies Using CFD and Comparison with Tip Loss Models. No. 7, 2004, pp. 343–356.